

# Manipulating the Exciton Dynamics in a MoS<sub>2</sub>/WS<sub>2</sub> Heterobilayer with a Si/Au Nanocavity

Shimei Liu, Shulei Li, Yuheng Mao, Zhenxu Lin, Mingcheng Panmai, Guang-Can Li, Lidan Zhou, and Sheng Lan\*

Manipulating the exciton dynamics in a heterobilayer (HB) composed of two transition metal dichalcogenides (TMDCs) is important in the development of photonic/plasmonic devices based on TMDC HBs. Here, the realization of such a manipulation in a MoS<sub>2</sub>/WS<sub>2</sub> HB is reported by using a Si/Au hybrid nanocavity composed of a Si nanoparticle and an Au film, which is manifested in the modification in the photoluminescence (PL) of the embedded MoS<sub>2</sub>/WS<sub>2</sub> HB. It is shown that a transition from PL quenching to PL enhancement can be achieved by adjusting the diameter of the Si nanoparticle, which modifies the plasmon resonance supported by the Si/Au nanocavity. More interestingly, it is demonstrated that the enhancement factor can be manipulated by shifting the exciton/trion resonance close to or far away from the plasmon resonance by simply increasing the laser power. It is revealed that the manipulation is realized by effectively controlling the strain and Purcell effects induced by the Si/Au nanocavity. A PL enhancement factor as large as  $\approx 187$  in the MoS<sub>2</sub>/WS<sub>2</sub> HB at a high laser power is observed. The findings suggest the potential applications of dielectric-metal hybrid nanocavities in the manipulation of the exciton dynamics in TMDC HBs and the development of novel plasmonic devices.

## 1. Introduction

2D transition-metal dichalcogenides (TMDCs), such as tungsten sulfide (WS<sub>2</sub>) and molybdenum sulfide (MoS<sub>2</sub>), are considered as promising candidates for light-harvesting and optoelectronic devices.<sup>[1,2]</sup> In general, a TMDC (MX<sub>2</sub>, M = Mo, W; X = S, Se, Te) monolayer is a semiconductor with direct bandgap, large exciton binding energy, and large optical absorption,<sup>[3–10]</sup> which implies highly efficient photoluminescence (PL). A heterobilayer (HB) created by stacking two TMDC monolayers offer us the opportunity for studying many exciting phenomena in 2D systems, such as Moiré patterns,<sup>[11–14]</sup> spintronics,<sup>[15]</sup> valleytronics,<sup>[16]</sup> and interlayer excitons.<sup>[17]</sup> In general, a TMDC HB possesses a type II energy band structure in which the carrier relaxation is dominated by interlayer charge transfer.<sup>[18]</sup> It means that the photogenerated electrons and holes are relaxed to the

conduction and valence band minima of different materials. Thus, the efficient separation of photogenerated electrons and holes leads to the quenching of the PL from TMDC HBs, limiting their applications in light emitting devices. So far, various strategies have been proposed to suppress the interlayer charge transfer and to enhance the PL from TMDC HBs. For example, it has been demonstrated that the interlayer charge transfer can be suppressed by placing an atomically thin charge-blocking layer, such as few-layer hexagonal boron nitride, in between the two TMDC monolayers.<sup>[19]</sup> In the absence of a charge-blocking interlayer, the PL enhancement can also be achieved if the nonradiative energy transfer from the material with a higher work function to that with a lower one in the TMDC HB dominates over the charge transfer process.<sup>[19–21]</sup>


Traditionally, the PL from a TMDC HB can be controlled by substrate, strain,<sup>[22,23]</sup> and temperature. It has been demonstrated that strain effect and high temperature would result in redshift and reduction in the PL of a WS<sub>2</sub> monolayer in the presence of Si nanoparticle.<sup>[24]</sup> The strain will induce the transition of a WS<sub>2</sub> monolayer from direct to indirect bandgap, leading to a similar modulation in the lattice vibration and PL emission. The non-uniform strain changes locally the conduction and valence bands of the WS<sub>2</sub> monolayer, attracting excitons and trions

S. Liu, Y. Mao, Z. Lin, G.-C. Li, S. Lan  
Guangdong Provincial Key Laboratory of Nanophotonic Functional Materials and Devices  
School of Information and Optoelectronic Science and Engineering  
South China Normal University  
Guangzhou 510006, P. R. China  
E-mail: slan@scnu.edu.cn

S. Li  
School of Optoelectronic Engineering  
Guangdong Polytechnic Normal University  
Guangzhou 510665, P. R. China

M. Panmai  
School of Electrical and Electronic Engineering  
Nanyang Technological University  
Singapore 639798, Singapore

L. Zhou  
State Key Laboratory of Optoelectronic Materials and Technologies  
School of Electronics and Information Technology  
Sun Yat-sen University  
Guangzhou 51006, P. R. China

 The ORCID identification number(s) for the author(s) of this article can be found under <https://doi.org/10.1002/lpor.202300850>

DOI: 10.1002/lpor.202300850

toward the point of maximum strain and achieving the efficient conversion of excitons and trions.<sup>[25]</sup> Additionally, the formation of interlayer excitons in a TMDC HB is closely related to the non-uniform interlayer coupling strength, which depends on interfacial contamination and local strain-induced deformation.<sup>[26,27]</sup> Very recently, it was shown that the competing emission rates of intra- and inter-layer excitons in a  $\text{WSe}_2/\text{Mo}_{0.5}\text{W}_{0.5}\text{Se}_2$  HB can be dynamically manipulated by controlling the interlayer distance with an Au tip.<sup>[27]</sup>

A variety of optical nanocavities have been proposed to enhance the light emission from a TMDC monolayer by controlling the local electric field.<sup>[28–31]</sup> On the other hand, plasmonic nanocavities are also employed to enhance the light emission of TMDC monolayers, relying mainly on the enhancement in the excitation rate, quantum efficiency, and emission directionality.<sup>[32,33]</sup> The enhancement in the quantum efficiency ( $\eta$ ) is determined by the Purcell factor, which is proportional to  $Q/V$ . Here,  $Q$  and  $V$  are the quality factor and mode volume of an optical nanocavity.<sup>[28,32]</sup> It is expected that the radiative recombination rate of intralayer excitons in a TMDC HB can be enhanced by the large Purcell factor of an optical/plasmonic nanocavity, leading to an enhancement in the PL of the TMDC HB.

All-metallic nanoparticles possess the advantages of small mode volume and large field enhancement.<sup>[34,35]</sup> However, the Ohmic loss originating from the large imaginary parts of metals in the visible light spectrum leads to severe heating of TMDCs.<sup>[36]</sup> Since  $\text{WS}_2$  monolayer has a small thermal conductivity at room temperature,<sup>[37]</sup> the accumulated heat will result in the PL quenching of the  $\text{WS}_2$  monolayer. In contrast, a dielectric-metal hybrid nanocavity composed of a high-index dielectric nanoparticle and a thin metal film can simultaneously achieve enhanced electric field, small mode volume, and negligible Ohmic loss.<sup>[38–41]</sup> A recent study reveals that the temperature in the gap region between the nanoparticle and the metal film is much lower in a dielectric-metal nanocavity ( $\text{Si}/\text{WS}_2/\text{Au}$ ) as compared with an all-metallic one ( $\text{Au}/\text{WS}_2/\text{Au}$ ).<sup>[42,43]</sup> It implies that the heat generated by laser irradiation in a dielectric-metal nanocavity can be greatly reduced. Therefore, it is expected that the PL quenching in a  $\text{MoS}_2/\text{WS}_2$  HB can be effectively suppressed when it is embedded into a  $\text{Si}/\text{Au}$  nanocavity. Recently, a reversible switch from exciton dissociation to exciton funneling, which is manifested as PL quenching and PL enhancement, was realized in a  $\text{MoSe}_2/\text{WS}_2$  HB by applying a gate voltage.<sup>[44]</sup> It has been known that the exciton resonances in many TMDCs can be easily tuned by laser irradiation.<sup>[45–47]</sup> Therefore, it is expected that the PL intensity of a TMDC HB can be dynamically controlled by laser irradiation.

In this article, we proposed the use of a  $\text{Si}/\text{Au}$  hybrid nanocavity to manipulate the exciton dynamics in a  $\text{MoS}_2/\text{WS}_2$  HB embedded into the  $\text{Si}/\text{Au}$  nanocavity. The PL intensity of the  $\text{MoS}_2/\text{WS}_2$  HB was modified by the strain effect induced by the adhesion force between the Si nanoparticle and the Au film and the Purcell effect induced by the plasmon mode supported by the  $\text{Si}/\text{Au}$  nanocavity. We examined the PL spectra of  $\text{Si}/\text{HB}/\text{Au}$  nanocavities composed of Si nanoparticles with different diameters. We demonstrated experimentally a transition from PL quenching to PL enhancement in the  $\text{MoS}_2/\text{WS}_2$  HB statically by adjusting the diameter of the Si nanoparticle and dynamically by changing the laser power.

## 2. Results and Discussion

### 2.1. Strain and Purcell Effects for a $\text{MoS}_2/\text{WS}_2$ HB Embedded in a $\text{Si}/\text{Au}$ Nanocavity

In Figure 1a, we show schematically a  $\text{Si}/\text{Au}$  hybrid nanocavity constructed with a Si nanoparticle and a thin Au film (or an  $\text{Au}/\text{SiO}_2$  substrate). A  $\text{MoS}_2/\text{WS}_2$  HB is embedded in the  $\text{Si}/\text{Au}$  nanocavity (see Experimental Section for the detailed fabrication process of the samples). For convenience, a  $\text{Si}/\text{Au}$  nanocavity with an embedded  $\text{MoS}_2/\text{WS}_2$  HB is denoted as  $\text{Si}/\text{HB}/\text{Au}$ . The  $\text{MoS}_2/\text{WS}_2$  HB attached on the  $\text{Au}/\text{SiO}_2$  substrate (in the absence of a Si nanoparticle), which is used as the reference sample, is denoted as  $\text{HB}/\text{Au}$ . Here, the  $\text{Si}/\text{Au}$  nanocavity is employed to manipulate the exciton dynamics and emission properties of the  $\text{MoS}_2/\text{WS}_2$  HB through the strain and Purcell effects.

It is well known that the combination of a  $\text{MoS}_2$  and a  $\text{WS}_2$  monolayer forms a type II heterostructure.<sup>[18]</sup> Upon the excitation of laser light, the electrons and holes generated in the  $\text{MoS}_2/\text{WS}_2$  HB will relax to the bottom of the conduction band in the  $\text{MoS}_2$  monolayer and the top of the valence band in the  $\text{WS}_2$  monolayer, respectively. The separation of electrons and holes in different materials after the optical excitation leads to the quenching of the PL from the  $\text{MoS}_2/\text{WS}_2$  HB, as shown in the inset in Figure 1a (see Note S1, Supporting Information), where an optical image obtained by using single-photon laser scanning confocal microscopy is presented. The large and bright triangle is  $\text{WS}_2$  monolayer while the small and dark ones are  $\text{MoS}_2/\text{WS}_2$  HBs. Previous studies indicate that the PL quenching of a  $\text{MoS}_2/\text{WS}_2$  HB is determined by the interlayer coupling strength, which is highly sensitive to the strain-induced deformation.<sup>[27]</sup> Therefore, it is expected that placing a Si nanoparticle on the  $\text{MoS}_2/\text{WS}_2$  HB will introduce a local strain on it, modifying the interlayer coupling strength via the deformation of the  $\text{MoS}_2$  monolayer, as schematically shown in Figure 1a. It should be emphasized, however, that the strain does not arise from the gravity of the Si nanoparticle, which is estimated to be only  $\approx 0.1$  fN. It originates from the adhesion forces between the Si nanoparticle and the Au film, which belongs to the van der Waals force. In the preparation of the samples, the aqueous solution of Si nanoparticles was dropped on the  $\text{MoS}_2/\text{WS}_2$  HB attached on the Au film and dried naturally. It is well known that hydrogen bond, which is a strong form of dipole-dipole attraction, can form between water molecules. As a result, a “long-range” intermolecular force may bridge two interacting atoms or molecules in the presence of water.<sup>[48]</sup> During the evaporation of water, the surface tension (a “long-range” intermolecular force) will bring the Si nanoparticle close to the Au film. Finally, the adhesion force between the Si nanoparticle and the Au film (van der Waals force) can reach an order of nN (see Note S2, Supporting Information),<sup>[49]</sup> which is large enough to induce a local deformation of the  $\text{MoS}_2$  monolayer and change the interlayer coupling strength.<sup>[27]</sup> Basically, the adhesion force of a metal-dielectric interaction is not influenced by the gap material (see Note S2, Supporting Information). We also evaluated the adhesion force between a Si nanoparticle and a  $\text{MoS}_2$  film (see Note S2, Supporting Information). It appeared to be larger than that between a Si nanoparticle and an Au film. As schematically depicted in Figure 1a, the strain induced by the Si nanoparticle

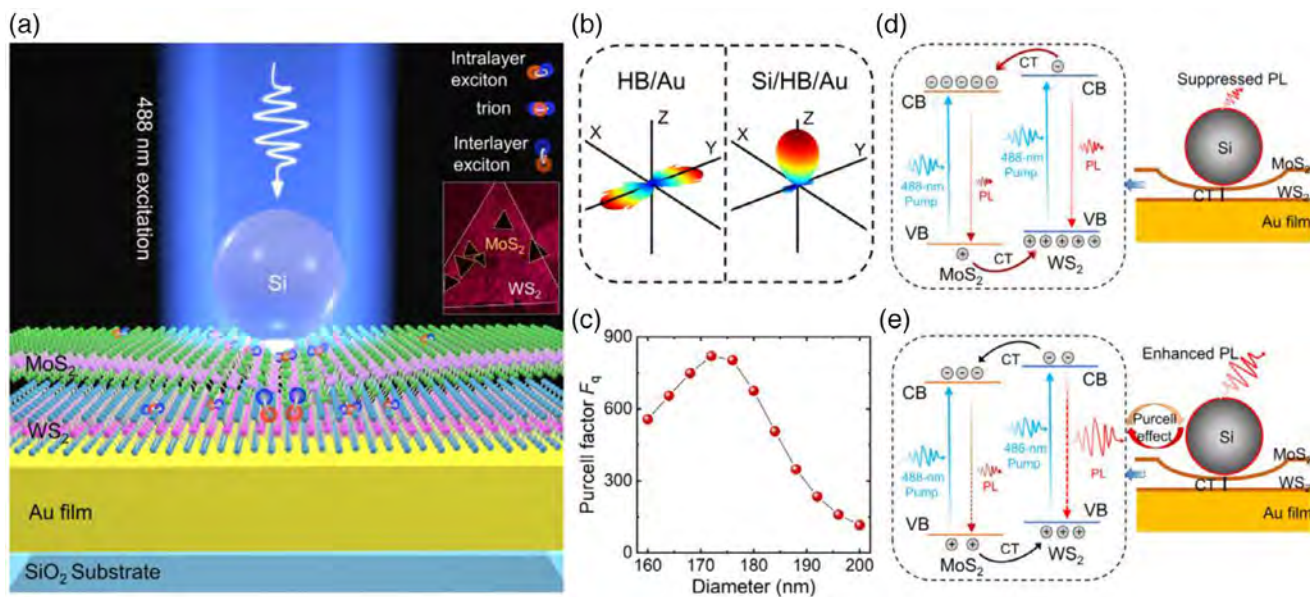


**Figure 1.** Strain and Purcell effects for a MoS<sub>2</sub>/WS<sub>2</sub> HB embedded in a Si/Au nanocavity. a) Schematic showing the manipulation of the exciton dynamics in a MoS<sub>2</sub>/WS<sub>2</sub> HB by using a Si/Au nanocavity. The PL mapping of MoS<sub>2</sub>/WS<sub>2</sub> HBs obtained by using a single-photon laser scanning confocal microscopy is shown in the inset. b) 3D radiation patterns calculated for a HB/Au and a Si/HB/Au nanocavity with  $d = 178$  nm. c) Purcell factors ( $F_q$ ) calculated for Si/Au nanocavities composed of Si nanoparticles with different diameters at the exciton resonance (615 nm) of WS<sub>2</sub> monolayer. d,e) Band diagram of a MoS<sub>2</sub>/WS<sub>2</sub> HB depicting the charge transfer (CT) and radiative combination of excitons occurring in a Si/HB/Au nanocavity, which leads to reduced and enhanced PL intensity respectively.

will reduce the interlayer distance and enhance the interlayer coupling strength, accelerating the interlayer charge transfer in the MoS<sub>2</sub>/WS<sub>2</sub> HB and resulting in a further PL quenching.<sup>[27]</sup>

From another viewpoint, the plasmon mode supported by the Si/Au nanocavity possesses a small mode volume, providing a strongly localized electric field in the gap between the Si nanoparticle and the Au film (see Note S3, Supporting Information). This plasmon mode is formed by the interaction between the electric dipole (ED) supported by the Si nanoparticle and the mirror image induced by the Au film, which is generally referred to as a mirror-image-induced magnetic dipole (MMD).<sup>[50,51]</sup> Due to the large gap width and the efficient charge transfer in the MoS<sub>2</sub>/WS<sub>2</sub> HB, the coupling between the plasmon mode and the exciton resonances is in the weak coupling regime,<sup>[42]</sup> where the Purcell effect is dominant. In this case, the radiative recombination rate of excitons is governed by the Purcell factor ( $F_q$ ),<sup>[52]</sup> which is defined as  $F_q \propto Q/V$ . Here,  $Q$  and  $V$  represent the quality factor and mode volume of the plasmon mode. Therefore, the PL intensity of the MoS<sub>2</sub>/WS<sub>2</sub> HB can be enhanced through the Purcell factor of the plasmon mode supported by the Si/Au nanocavity. Since most excitons in the MoS<sub>2</sub>/WS<sub>2</sub> HB are horizontally oriented, they are influenced only by the in-plane electric field ( $E_{xy}$ ) of the plasmon mode. For this reason, we first examined the wavelength-dependent enhancement factors of the in-plane electric field ( $\int |E_{xy}(\lambda)|^2 dV/V$ ) averaged over the volume of the MoS<sub>2</sub>/WS<sub>2</sub> HB (see Figure S3c,d, Supporting Information). The thickness of the MoS<sub>2</sub>/WS<sub>2</sub> HB was assumed to be  $t = 2.0$  nm. Then, we simulated the 3D radiation patterns of a dipole source located on the HB/Au and Si/HB/Au nanocavity, respectively. The results are shown in Figure 1b (see Figure S3e,f, Supporting Information). It is noticed that the radiation intensity and pat-

tern of the dipole source are dramatically modified in the presence of the Si/Au nanocavity. In Figure 1c, we present the Purcell factors calculated for the plasmon modes supported by different Si/Au nanocavities (i.e., Si/Au nanocavities composed of Si nanoparticles with different diameters ( $d$ )) at the exciton resonance (615 nm) (see Experimental Section for details). It was found that the largest Purcell factor ( $\approx 803$ ) is obtained in the Si/Au nanocavity with  $d \approx 178$  nm. In this case, the plasmon mode supported by the Si/Au is resonant with the exciton resonance ( $\approx 615$  nm) in the WS<sub>2</sub> monolayer, leading to the largest enhancement in the PL intensity.

For a MoS<sub>2</sub>/WS<sub>2</sub> HB embedded in a Si/Au nanocavity, the charge transfer will be facilitated by the strain induced by the Si nanoparticle, leading to the PL quenching. On the other hand, the radiative combination of excitons can be accelerated by the Purcell effect, leading to the PL enhancement. The competition between these two effects offers us the opportunity for manipulating the PL intensity of the MoS<sub>2</sub>/WS<sub>2</sub> HB by varying the plasmon mode through the change in the diameter of the Si nanoparticle. When the MMD mode is far away from the exciton resonance, the exciton dynamics are dominated by the efficient charge transfer induced by the strain effect. As a result, a reduced PL is observed in the presence of the Si nanoparticle, as depicted in Figure 1d. For a Si/Au nanocavity supporting a plasmon mode close to the exciton resonance, the PL enhancement resulting from the Purcell effect may counteract or even surpass the PL quenching originating from the charge transfer. In this case, the exciton dynamics is governed by the radiative recombination of excitons, as depicted in Figure 1e. Therefore, we can achieve either a reduced or an enhanced PL from a MoS<sub>2</sub>/WS<sub>2</sub> HB by simply adjusting the diameter of the Si nanoparticle.

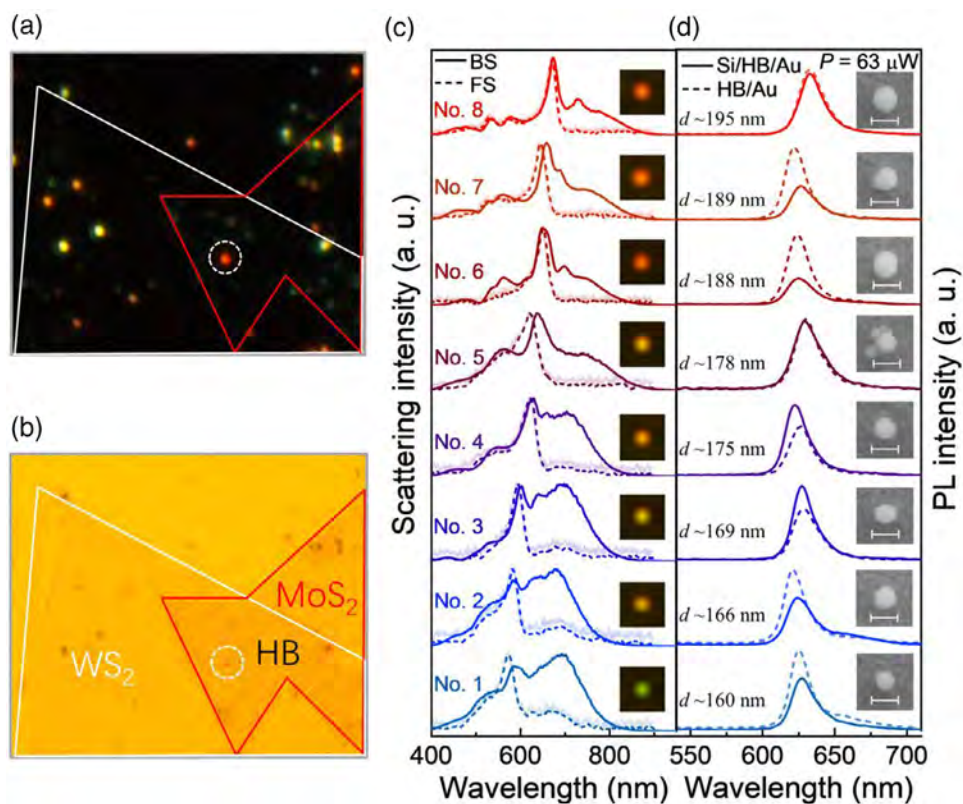


**Figure 2.** Manipulating the PL of a MoS<sub>2</sub>/WS<sub>2</sub> HB by adjusting the diameter of the Si nanoparticle. a) b) The dark- and bright-field images of a HB/Au and Si nanoparticles. A Si nanoparticle used to construct a Si/HB/Au nanocavity is enclosed by the dashed circle in Figure 2a,b). In Figure 2c, we present the forward and backward scattering spectra measured for Si/HB/Au nanocavities composed of Si nanoparticles with different diameters. The CCD images of the corresponding forward scattering light are shown in the insets. In each case, the MMD mode supported by the nanocavity is manifested as a scattering peak in the forward scattering spectrum. The resonant wavelength of the plasmon mode is redshifted from  $\approx 583$  to  $\approx 673$  nm with increasing the diameter of the Si nanoparticle. Accordingly, the scattering light of the Si nanoparticle is changed gradually from green to orange and finally to red (see the CCD images in the insets). d) PL spectra measured for Si/HB/Au nanocavities composed of Si nanoparticles with different diameters at  $P = 63 \mu\text{W}$  (solid curves). The PL spectra of the HB/Au measured at  $P = 63 \mu\text{W}$  (dashed curves) are also provided for comparison. The SEM images of the Si nanoparticles are shown in the insets. The length of the scale bar is 200 nm. The diameters of the Si nanoparticles were estimated based on the SEM images.

## 2.2. Manipulating the PL of a MoS<sub>2</sub>/WS<sub>2</sub> HB by Adjusting the Diameter of the Si Nanoparticle

Figure 2a,b show the dark- and bright-field images of a MoS<sub>2</sub>/WS<sub>2</sub> HB formed on a thin Au film (see Note S4, Supporting Information). It is obtained by first transferring a WS<sub>2</sub> monolayer grown by chemical vapor deposition (CVD) onto a thin Au film (an Au/SiO<sub>2</sub> substrate). Then, a MoS<sub>2</sub> monolayer grown by CVD was transferred onto the WS<sub>2</sub> monolayer, forming a MoS<sub>2</sub>/WS<sub>2</sub> HB (see Experimental Section). In this work, the interlayer coupling and formation of interlayer excitons in the MoS<sub>2</sub>/WS<sub>2</sub> HBs may be affected by the residual polymer used in the transfer process. This is the reason why the emission from interlayer excitons was not revealed in the PL spectra of the MoS<sub>2</sub>/WS<sub>2</sub> HBs, similar to that reported in literature.<sup>[26]</sup> In fact, the interlayer coupling can be improved to observe the interlayer excitons by adding an annealing process for the MoS<sub>2</sub>/WS<sub>2</sub> HBs. We performed atomic force microscopy (AFM) characterization for the MoS<sub>2</sub>/WS<sub>2</sub> HBs. It was found that the typical interlayer distance between the MoS<sub>2</sub> and WS<sub>2</sub> monolayers was similar to that reported in literature (see Note S5, Supporting Information).<sup>[18]</sup> Based on the scanning electron microscopy (SEM) observations and Raman spectra measurements (see Note

S5, Supporting Information), we didn't find any strains, grain boundaries and defects in the MoS<sub>2</sub>/WS<sub>2</sub> HBs. In Figure 2a, one can identify a Si nanoparticle located on the MoS<sub>2</sub>/WS<sub>2</sub> HB, which exhibits red scattering light (enclosed by a dashed circle in Figure 2a,b). In Figure 2c, we present the forward and backward scattering spectra measured for eight Si/HB/Au nanocavities composed of Si nanoparticles with different diameters (see Note S6, Supporting Information). The images of the forward scattering light recorded by using a charge coupled device (CCD) are shown in the insets. In each case, the MMD mode supported by the nanocavity is manifested as a scattering peak in the forward scattering spectrum. The resonant wavelength of the plasmon mode is redshifted from  $\approx 583$  to  $\approx 673$  nm with increasing the diameter of the Si nanoparticle. Accordingly, the scattering light of the Si nanoparticle is changed gradually from green to orange and finally to red (see the CCD images in the insets).

In Figure 2d, we present the PL spectra measured for the eight Si/HB/Au nanocavities (see Note S7, Supporting Information). In each case, the PL spectrum measured for the adjacent HB/Au is also provided for reference. Since the PL intensity of the MoS<sub>2</sub>/WS<sub>2</sub> HB is dominated by the PL of the WS<sub>2</sub> monolayer (see Note S1, Supporting Information), the PL manipulation of

the MoS<sub>2</sub>/WS<sub>2</sub> HB is realized mainly by controlling the PL of the WS<sub>2</sub> monolayer. Compared to the previous work,<sup>[43]</sup> the laser power used in this work is much lower (with a maximum laser power of 1.26 mW). In addition, the absorption of MoS<sub>2</sub> monolayer ( $\approx 8\%$ ) is also much smaller than that of WS<sub>2</sub> monolayer ( $\approx 17\%$ ).<sup>[10]</sup> Therefore, the change in the dielectric constant of MoS<sub>2</sub> monolayer induced by laser irradiation is relatively small. Moreover, the interlayer charge transfer in the MoS<sub>2</sub>/WS<sub>2</sub> HB is an ultrafast process ( $\approx 50$  fs).<sup>[18]</sup> Thus, the modulation in the PL intensity of the WS<sub>2</sub> monolayer caused by the small variation in the dielectric constant of the MoS<sub>2</sub> monolayer is negligible. In the PL measurements, a moderate laser power ( $P = 63 \mu\text{W}$ ) was employed in order to suppress the thermal effects induced by laser irradiation. For nanocavities containing small Si nanoparticles (see Nos. 1 and 2), the plasmon mode (MMD) is located on the short-wavelength side of the exciton resonance of WS<sub>2</sub> monolayer ( $\approx 615$  nm). In this case, we observed the reduced PL from the MoS<sub>2</sub>/WS<sub>2</sub> HB embedded in the nanocavities. In a previous study, it was found that the area influenced by the strain induced with a Si nanoparticle was estimated to be  $\approx 0.7 \times 0.7 \mu\text{m}^2$ , which is close to the size of the laser spot ( $\approx 1.2 \times 1.2 \mu\text{m}^2$ ).<sup>[24]</sup> Since the plasmon mode is far away from the exciton resonance, the exciton dynamics are dominated by the charge transfer facilitated by the strain, leading to a reduced PL intensity. When the plasmon mode is close to the exciton resonance, an enhanced PL intensity is observed (see Nos. 3 and 4). In this case, the radiative recombination rate of excitons is greatly enhanced by the large Purcell factor provided by the nanocavity, resulting in an enhancement in the PL intensity. More electrons and holes recombine radiatively in the form of excitons before they are relaxed to the minima of the conduction and valence bands. In order to gain a deep insight into the influence of a Si/Au nanocavity on the exciton dynamics in an embedded MoS<sub>2</sub>/WS<sub>2</sub> HB, we carried out PL lifetime measurements for some Si/HB/Au nanocavities exhibiting enhanced PL intensities (see Note S8, Supporting Information and Experimental Section). It was found that the PL lifetime is reduced as compared with the reference HB due to the Purcell effect. As mentioned above, the strain arises from the adhesion force between the Si nanoparticle and the Au film. It is not sensitive to the diameter of the Si nanoparticle, which is in the range of 150–200 nm (see Note S2, Supporting Information). When the plasmon mode is shifted to a longer wavelength of the exciton resonance (see No. 5), the Purcell effect is reduced rapidly. In this case, the PL quenching induced by the strain effect is balanced by the PL enhancement caused by the Purcell effect. As a result, the PL intensity in the presence of the nanocavity remains almost unchanged. For nanocavities composed of Si nanoparticles with larger diameters (see Nos. 6 and 7), the plasmon mode is further shifted to a longer wavelength, which is far away from the exciton resonance. In this case, the Purcell effect becomes weaker while the strain effect becomes stronger. Thus, we observed a significantly reduced PL intensity in the presence of the nanocavity. For the largest nanoparticle (No. 8), it exhibits a negligible reduction in the PL intensity. Since the strain induced by a nanoparticle is quite sensitive to the morphology of the nanoparticle, we speculate that the strain induced by this nanoparticle is small due to the non-spherical shape. Therefore, we demonstrated that the PL quenching in a MoS<sub>2</sub>/WS<sub>2</sub> HB caused by the charge transfer can be overcome by the Purcell effect induced by a Si/Au nanocavity

with an appropriate size, leading to an enhancement in the PL intensity. The manipulation of the PL intensity can be realized by simply adjusting the diameter of the Si nanoparticle used to construct the nanocavity.

### 2.3. Reduced PL Intensity Induced by the Strain Effect in a Si/Au Nanocavity

It has been demonstrated that the PL intensity of the MoS<sub>2</sub>/WS<sub>2</sub> HB can be dramatically reduced by using a Si/Au nanocavity composed of a Si nanoparticle with a larger diameter (e.g., Nos. 6 and 7) (see Notes 7 and 9, Supporting Information). In Figure 3a, we present the PL spectra of such a Si/HB/Au nanocavity measured at different laser powers. In each case, the PL spectrum of the reference sample (i.e., HB/Au) is also provided for comparison. With increasing the laser power, the reduction in the PL intensity becomes significant. In addition, one can observe a redshift of the PL peak and a broadening of the linewidth. The redshift of the PL peak is found to be  $\approx 16$  nm at a high laser power of  $P = 1.26$  mW (see Note S10, Supporting Information). The reduction of the PL intensity can be characterized by relative PL intensity defined as  $(I-I_0)/I_0$ , where  $I$  and  $I_0$  represent the PL intensities of the Si/HB/Au and HB/Au. In Figure 3b, we summarize the relative PL intensities of three Si/HB/Au nanocavities (Nos. 1, 6, and 7) at different laser powers (see Note S11, Supporting Information). In each case, one can see a rapid decrease of the relative PL intensity with increasing laser power. It becomes saturated at high laser powers. The minimum relative PL intensity reaches  $\approx -84\%$ . Basically, a temperature rise in the Si/HB/Au is anticipated with increasing laser power due to the non-radiative recombination of excitons. It will accelerate the carrier relaxation or the separation of electrons and holes, leading to the quenching of the PL intensity. The WS<sub>2</sub> monolayer in contact with the Au film possesses a low thermal conductivity, leading to the accumulation of the heat.<sup>[53]</sup> Thus, temperature in the Si/HB/Au nanocavity will rise quickly at high laser powers. In Figure 3c, we show the dependence of the integrated PL intensity on the laser power for a Si/HB/Au nanocavity (No. 7), which is plotted in a logarithmic coordinate. A slope of  $\approx 0.91$  is extracted for the Si/HB/Au nanocavity based on the fitting of the experimental data. This value is smaller than the slope ( $\approx 0.99$ ) observed for the HB/Au, indicating the PL quenching induced by the temperature rise. In Figure 3d, we show the ratio of the emission intensity of trions ( $I_t$ ) to that of excitons ( $I_e$ ) as a function of the laser power observed for this nanocavity. It can be seen that the ratio ( $I_t/I_e$ ) in the Si/HB/Au nanocavity increases rapidly with increasing laser power and it becomes much larger than that in the HB/Au at high laser powers. This behavior implies the efficient conversion of excitons to trions induced by the non-uniform strain in the Si/HB/Au nanocavity.<sup>[25,54]</sup>

### 2.4. Manipulating the PL Intensity of a Si/HB/Au Nanocavity by Changing Laser Power

As demonstrated above, the PL intensity of a MoS<sub>2</sub>/WS<sub>2</sub> HB can be modified by exploiting the Purcell effect of the plasmon mode supported by a Si/Au nanocavity. The largest Purcell factor is

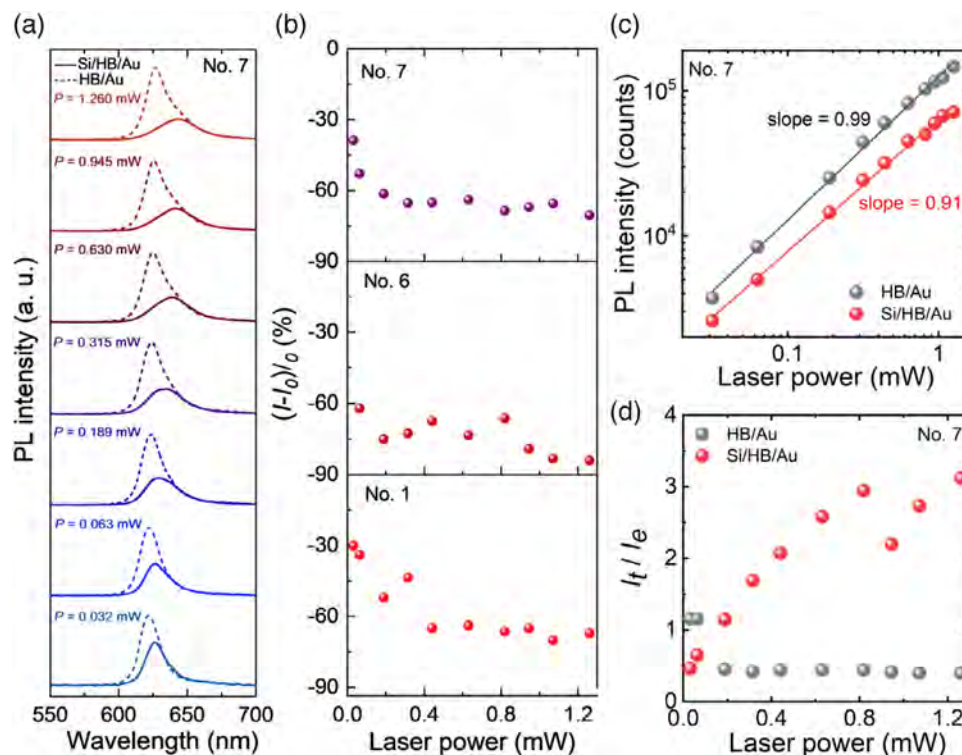


**Figure 3.** Reduced PL intensity induced by the strain effect in a Si/HB/Au nanocavity. a) PL spectra measured for a Si/HB/Au nanocavity (No. 7) at different laser powers. The PL spectra of the nearby HB/Au measured under the same conditions are provided for comparison. b) Dependences of the relative PL intensities  $((I-I_0)/I_0)$  on the laser power observed for three Si/HB/Au nanocavities (Nos. 1, 6, and 7). c) Dependence of the integrated PL intensity on the laser power observed for the Si/HB/Au nanocavity (No. 7) and HB/Au. d) Dependence of the intensity ratio  $(I_t/I_e)$  on the laser power observed for the Si/HB/Au nanocavity (No. 7) and HB/Au.

achieved at the plasmon resonance. Thus, the energy difference between the plasmon resonance and the exciton resonance plays a crucial role in determining the PL intensity of the MoS<sub>2</sub>/WS<sub>2</sub> HB. It has been demonstrated that the PL intensity of the MoS<sub>2</sub>/WS<sub>2</sub> HB can be manipulated by tuning the plasmon resonance of the Si/Au nanocavity via the change in the diameter of the Si nanoparticle. For practical applications, it is highly desirable that the PL manipulation can be realized in a Si/HB/Au through the change of excitation condition. Previous studies indicate that the exciton resonance of a WS<sub>2</sub> monolayer can be shifted to longer wavelengths by simply increasing the excitation laser power. In addition, charge excitons (trions) emerge at high laser powers and they also exhibit a redshift with increasing the laser power.<sup>[45,46]</sup> This unique feature offers us the opportunity for modifying the energy detuning between the plasmon resonance and the exciton/trion resonance, changing dynamically the PL intensity of the Si/HB/Au nanocavity. In **Figure 4a**, we present the wavelength shifts of the excitons and trions induced by increasing the laser power for three typical Si/HB/Au nanocavities (Nos. 3, 4, and 5), whose plasmon resonances are close to the exciton resonance. In each case, the resonant wavelengths of excitons and trions are extracted by fitting the PL spectrum with Lorentz lineshapes (see Note S7, Supporting Information). The PL intensities of excitons and trions, which are denoted as  $I_e$  and  $I_t$ , are also obtained from the fitting results (see Note S12, Supporting Information). As expected, the exciton and trion resonances are shifted to longer wavelengths with increas-

ing laser power in all cases. For the small Si/HB/Au nanocavity (No. 3), the plasmon resonance ( $\approx 600.4$  nm) is located at the short-wavelength side of the exciton/trion resonance in the absence of laser excitation. For the moderate Si/HB/Au nanocavity (No. 4), the plasmon resonance ( $\approx 626.3$  nm) coincides with the trion resonance at low laser powers. The plasmon resonance ( $\approx 637.7$  nm) of the large Si/HB/Au nanocavity (No. 5) appears at the long-wavelength side of the trion resonance. With increasing laser power, it is noticed that the exciton/trion resonance in the small Si/HB/Au nanocavity moves away from the plasmon resonance. In the moderate Si/HB/Au nanocavity, the exciton resonance moves toward the plasmon resonance while the trion resonance leaves rapidly away from the plasmon resonance. The redshift of the exciton resonance is small in the large Si/HB/Au nanocavity. In contrast, the trion resonance moves across the plasmon resonance rapidly and leaves gradually. As can be seen in the following, the PL enhancement or reduction induced by increasing the laser power is determined by the relative position of the exciton/trion resonance with respect to the plasmon resonance and the intensity ratio  $I_t/I_e$ . In **Figure 4b**, we present the dependence of the intensity ratio  $I_t/I_e$  on the laser power for the three Si/HB/Au nanocavities. In each case, the intensity ratio obtained for the HB/Au is also provided. In all cases, the intensity ratio  $I_t/I_e$  of the HB/Au increases linearly with increasing the laser power. For the small and large Si/HB/Au nanocavities, a similar trend is observed. In the small nanocavity, it is easily understood because the exciton/trion resonance is far away from

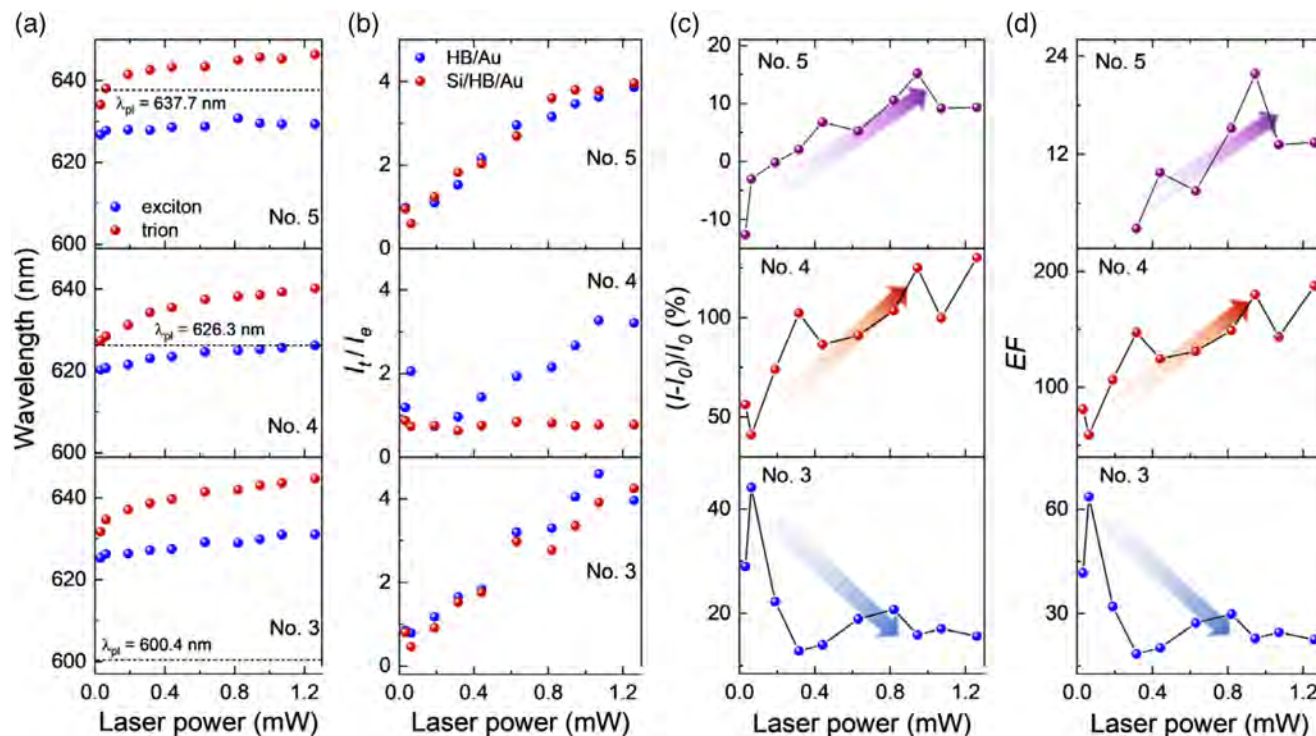


**Figure 4.** Manipulating the PL intensity of a Si/HB/Au nanocavity by changing laser power. a) Evolutions of the resonant wavelengths of excitons and trions with increasing laser power observed in three Si/HB/Au nanocavities (Nos. 3, 4, and 5). b) Evolutions of the intensity ratio ( $I_t/I_e$ ) with increasing laser power observed in three Si/HB/Au nanocavities. c) Dependence of the relative PL intensity ( $(I-I_0)/I_0$ ) on the laser power observed in three Si/HB/Au nanocavities. d) Dependence of the PL enhancement factor ( $EF$ ) on the laser power observed in three Si/HB/Au nanocavities.

the plasmon resonance and the influence of the plasmon mode is negligible. For the large nanocavity, a sublinear behavior is observed at high laser powers because the exciton resonance moves toward the plasmon resonance while the trion resonance moves away. It is interesting to notice that the intensity ratio  $I_t/I_e$  remains almost unchanged with increasing the laser power in the moderate nanocavity. This is caused by the rapid increase of the exciton intensity with increasing the laser power because the exciton resonance approaches the plasmon resonance at high laser powers. As a result, the conversion of excitons to trions is suppressed by the rapid recombination of excitons. In Figure 4c, the enhanced and reduced PL intensities are characterized by using the relative intensities of the Si/HB/Au nanocavities ( $I$ ) with respect to those of the HB/Au ( $I_0$ ). In the small nanocavity, we observe a rapid decrease of the relative intensity from  $\approx 44\%$  to  $\approx 15\%$  with the laser power raised to  $P = 0.3$  mW. After that, the change in the relative intensity is not obvious with increasing the laser power. For the moderate nanocavity, one can see a fast increase of the relative intensity from  $\approx 40\%$  to  $\approx 130\%$  when the laser power is increased to  $P = 1.26$  mW. It is beneficial from the redshift of the exciton resonance to the plasmon resonance induced by laser irradiation. In the large nanocavity, a transition from reduced PL ( $\approx -12\%$ ) to enhanced PL ( $\approx 15\%$ ) is realized by simply increasing the laser power. Although a large enhancement factor is achieved in the hot spot, the overall PL enhancement is not significant because the hot spot ( $\approx 0.0078 \mu\text{m}^2$ ) is much smaller as compared with the laser spot ( $\approx 1.13 \mu\text{m}^2$ ) (see Figure S3a, Supporting Information). In principle, we

can derive the PL enhancement factor in the hot spot by using the following formula:

$$EF = \frac{I - I_0}{I_0} \frac{S_0}{S_{NP}} \quad (1)$$

where  $S_0$  is the area of the laser spot ( $\approx 1.13 \mu\text{m}^2$ ),  $S_{NP}$  is the area of the hotspot. The dependence of the PL enhancement factor on the laser power derived for different nanocavities is shown in Figure 4d. It is interesting to notice that the PL enhancement factor of a Si/HB/Au can be modified by simple changing the laser power and an enhancement factor as large as  $\approx 187$  can be achieved in the moderate nanocavity at a laser power of  $P = 1.26$  mW.

### 2.5. Modifying the Emission Properties of a $\text{MoS}_2/\text{WS}_2$ HB by using a Si/Au Nanocavity

Apart from the Purcell effect induced by the plasmon mode of a Si/Au nanocavity, the emission properties of a  $\text{MoS}_2/\text{WS}_2$  HB can also be modified by the radiation behavior of the Si/Au nanocavity. In our case, the PL of the  $\text{MoS}_2/\text{WS}_2$  HB around the hot spot is first coupled to the Si/Au nanocavity and then emitted into the far field. Thus, the Si/Au nanocavity acts as a nano-antenna which influences the collection efficiency of the PL. This feature is reflected in the backward scattering spectrum of the Si/Au nanocavity. In Figure 5a, we show the backward scattering

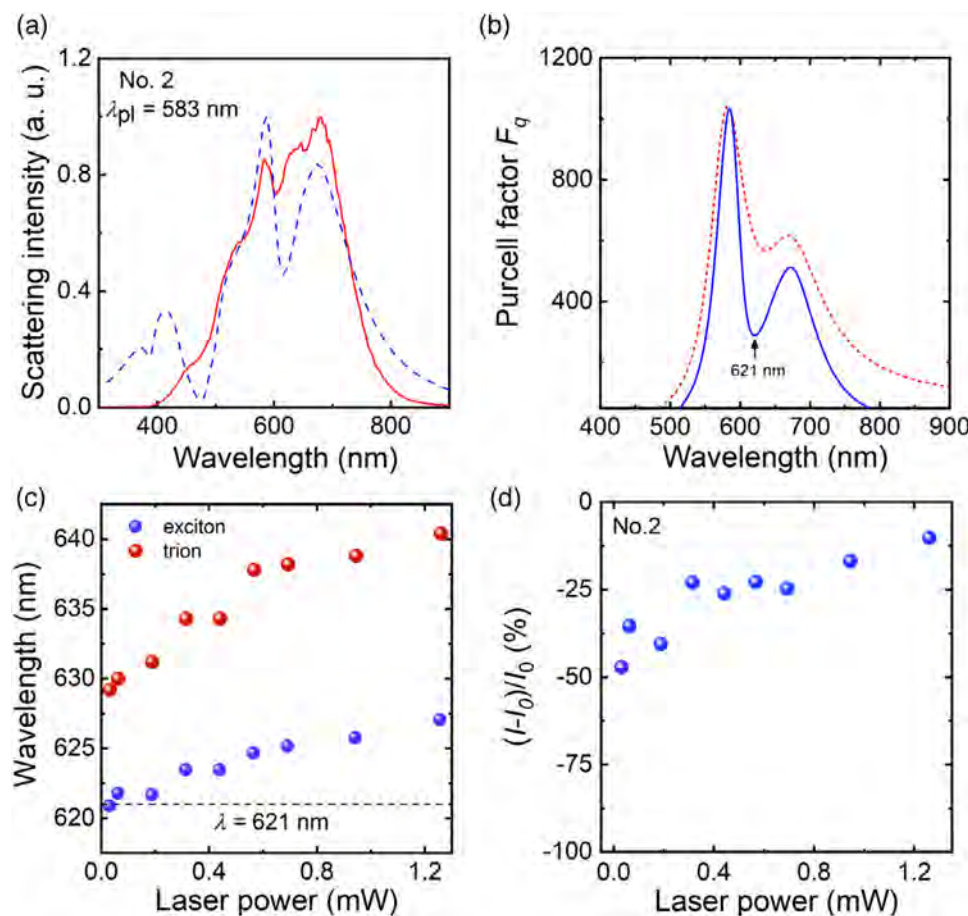


**Figure 5.** Modifying the emission properties of a  $\text{MoS}_2/\text{WS}_2$  HB by using a Si/Au nanocavity. a) Backward scattering spectrum (red solid curve) measured for a Si/HB/Au nanocavity (No. 2). The backward scattering spectrum (blue dashed curve) calculated for a Si/HB/Au nanocavity with  $d = 159$  nm is also provided for comparison. b) Purcell factors ( $F_q$ ) calculated for a Si/Au nanocavity with  $d = 159$  nm at different wavelengths (red dashed curve). Also shown is the wavelength dependent Purcell factors modified by the emission properties of the Si/Au nanocavity ( $d = 159$  nm) (blue solid curve). The wavelength highlighted (621 nm) indicates the wavelength above which the PL intensity will be enhanced by the other optical resonance. c) Dependences of the resonant wavelengths of excitons and trions on the laser power observed in the Si/HB/Au nanocavity (No. 2). The horizontal dashed line (621 nm) indicates the wavelength above which the PL intensity will be enhanced by the other optical resonance. d) Dependence of the relative PL intensity ( $(I-I_0)/I_0$ ) on the laser power observed in the Si/HB/Au nanocavity (No. 2).

spectrum measured for a Si/HB/Au nanocavity (No. 2). The calculated scattering spectrum is also provided for comparison. For the Si/Au nanocavities studied in this work, they usually support two optical modes which originate from the interference between the ED and MD modes excited in the Si nanoparticle with their mirror images induced by the Au film. The quality factor of the MMD mode, which is formed by the interaction between the ED mode and its mirror image, is larger because the ED and its mirror image are anti-parallel. In Figure 5b, we show the wavelength-dependent Purcell factor calculated for the nanocavity (red dashed curve). One can identify two maxima corresponding to the two plasmon modes supported by the nanocavity. The spectrum of the Purcell factor will determine the PL enhancement at different wavelengths. On the other hand, the collection efficiency of the PL is influenced by the backward scattering of the nanocavity.

In this work, we employed the Purcell effect induced by the MMD mode to modify the exciton dynamics in the  $\text{MoS}_2/\text{WS}_2$  HB. When the exciton/trion resonances are close to the MMD

mode, the other optical mode formed by the interference between MD and its image usually appears at a wavelength larger than 700 nm. Therefore, its influence on the exciton dynamics is negligible. For the small Si/Au nanocavities studied in this work (for example No. 2), the MMD mode locates at  $\approx 583$  nm while the other optical mode appears at  $\approx 674$  nm. With increasing laser power, the trion resonance of the  $\text{WS}_2$  monolayer is shifted toward this optical resonance (see Figure 5c). Based on the Purcell factor calculated for the Si/Au nanocavity, it is expected that the PL intensity of the  $\text{MoS}_2/\text{WS}_2$  HB increases only slightly with increasing laser power (see the red dashed curve in Figure 5b). However, the increase in the PL intensity of the Si/HB/Au nanocavity is significant (see Figure 5d). When we calculated the Purcell factor, only the mode volume and linewidth of the nanocavity were taken into account. The radiation of the Si/Au nanocavity, which is manifested in the backward scattering spectrum, was not considered. If the spectrum of the Purcell factor is multiplied by the calculated backward scattering spectrum, one can see clearly an increase of the PL intensity when



the trion resonance of  $WS_2$  is shifted to a longer wavelength (see the blue solid curve in Figure 5b). Thus, the PL intensity is eventually determined by the spectrum of the Purcell factor modified by the calculated backward scattering spectrum in Figure 5a (blue dashed curve). Similarly, we can shift the exciton and trion resonances of the  $WS_2$  monolayer by increasing the laser power, as shown in Figure 5c. Based on the modified spectrum of the Purcell factor shown in Figure 5b, one can expect an increase in the relative intensity with increasing the laser power. This prediction is in good agreement with the experimental observation shown in Figure 5d, where a gradual increase of the relative intensity from  $-47\%$  to  $-10\%$  is confirmed. Therefore, it is verified that the PL intensity of a  $MoS_2/WS_2$  HB can also be modified by the radiation properties of a Si/HB/Au nanocavity, which serves as a nano-antenna.

### 3. Conclusions

In summary, we have investigated systematically the manipulation of the exciton dynamics in a  $MoS_2/WS_2$  HB by using a Si/Au nanocavity. It is found that PL intensity of a Si/HB/Au nanocavity depends strongly on the diameter of the Si nanoparticle used to construct the nanocavity. The strain effect induced by Si nanoparticles facilitates the interlayer charge transfer, resulting in a serious PL quenching. In contrast, the large Purcell factor offered by a Si/Au nanocavity accelerates the radiative recombination rate of excitons, leading to the enhancement of PL intensity. We obtained the PL enhancement or reduction in a Si/HB/Au nanocavity by adjusting the diameter of the Si nanoparticle. Moreover, we demonstrated the PL manipulation of a Si/HB/Au nanocavity by changing the excitation laser power. As a research work in the near future, the absorption/differential reflectivity spectra of the Si/HB/Au system under simultaneous laser irradiation can be employed to realize the optical manipulation of the exciton dynamics. The manipulation of the exciton dynamics in a  $MoS_2/WS_2$  HB demonstrated in this work suggests the potential applications of dielectric-metal hybrid nanocavities in the construction of plasmonic devices.

### 4. Experimental Section

**Sample Preparation:** In this work, a wet-transfer approach was employed to transfer the  $WS_2$  and  $MoS_2$  monolayers grown by CVD sequentially onto the Au/SiO<sub>2</sub> substrate, creating the  $MoS_2/WS_2$  HBs. First, a thin film of poly(methyl methacrylate) (PMMA) was spin-coated on  $WS_2$  monolayers grown on a SiO<sub>2</sub>/Si substrate. Then, the PMMA/ $WS_2$  film was separated from the SiO<sub>2</sub>/Si substrate by etching with KOH (2 mol L<sup>-1</sup>) at 80°C. After removing the residual KOH by deionized water, PMMA/ $WS_2$  film was transferred onto an Au/SiO<sub>2</sub> substrate and soaked in acetone to dissolve the PMMA, obtaining  $WS_2$  monolayers on the Au/SiO<sub>2</sub> substrate. Finally,  $MoS_2$  monolayers were transferred onto the  $WS_2$  monolayers by using the same procedure, creating the  $MoS_2/WS_2$  HBs on the Au/SiO<sub>2</sub> substrate used in our study. Spherical Si nanoparticles with different diameters were fabricated by using femtosecond laser ablation.<sup>[55]</sup> The 800-nm femtosecond laser pulses (Legend. Coherent) with a duration of 100 fs and a repetition rate of 1 kHz were employed to ablate the Si wafer immersed in deionized water. The aqueous solution of Si nanoparticles was dropped on  $MoS_2/WS_2$  HBs and dried naturally, obtaining Si/HB/Au nanocavities operating at different wavelengths.

**Optical Characterization:** The forward and backward scattering spectra of Si/HB/Au nanocavities were measured by using a dark-field microscope

(Axio Observer A1. Zeiss) equipped with a color charge coupled device (CCD) (DS-Ri2, Nikon) and a spectrometer (SR-5001-B1, Andor). For the PL measurements, a 488-nm continuous wave laser beam was introduced into the microscope and focused on Si/HB/Au nanocavities or HB/Au ( $MoS_2/WS_2/Au$ ) by using a 50× objective. The PL intensity mapping was performed by using a single-photon laser scanning confocal microscopy operating at 488-nm. Time-resolved PL measurements were carried out by using an objective scanning confocal microscope system (MicroTime 200, PicoQuant) coupled with an inverted fluorescence microscope (IX71, Olympus). 405-nm circularly polarized laser light with pulse width of 55 ps and repetition rate of 40 MHz was used to excite Si/HB/Au and HB/Au through an oil-immersed objective (100×, NA = 1.4, Olympus). The emission from Si/HB/Au or HB/Au was collected by using the same objective and detected by a single photon avalanche photodiode (PDM 50CT, Micro Photon Devices) after passing a dichroic beam splitter (405rdc, Chroma) and a long-pass filter (HQ430CP, Chroma).

**Numerical Simulations:** In this work, the numerical simulations were performed by using the finite-difference time-domain technique. The dielectric constants of Au and Si were taken from Johnson and Christy<sup>[56]</sup> and from Palik,<sup>[57]</sup> respectively. The dielectric constants of  $MoS_2$  and  $WS_2$  monolayers were obtained from literature.<sup>[10]</sup> The refractive index of the surrounding media was chosen to be 1.0. In the calculation, the thickness of the  $MoS_2$  and  $WS_2$  monolayers was chosen to be 1.0 nm. A mesh size as small as 0.5 nm was used in the gap region between the Si nanoparticle and the Au film to ensure the convergence of numerical simulations and the achievement of accurate results. 3D radiation patterns were simulated by using a dipole source (615 nm) polarized along the x direction. The size of simulation area was set to 3.8 μm.

**Purcell Factor:** The Purcell factor of a 3D resonator is expressed as follows:<sup>[58]</sup>

$$F_q = \frac{3c^3}{4\pi^2\nu^2V} \frac{\Delta\nu_q}{4(\nu - \nu_q)^2 + \Delta\nu_q^2} \quad (2)$$

where  $\nu$ ,  $\nu_q$ , and  $V$  represent the frequency of the emitter, the frequency and mode volume of the resonator, respectively. If the frequency  $\nu_q$  of the resonator matches the frequency of the emitter  $\nu$ , the above equation can be approximated as follows:<sup>[58]</sup>

$$F_q = \frac{3\lambda_q^3 Q}{4\pi^2 V} \quad (3)$$

where  $Q$  represents the quality factor of the resonator. The mode volume of the resonator can be written as:<sup>[59]</sup>

$$V = \frac{\int \epsilon(\vec{r}) |\vec{E}(\vec{r})|^2 d^3\vec{r}}{\max(\epsilon(\vec{r}) |\vec{E}(\vec{r})|^2)} \quad (4)$$

### Supporting Information

Supporting Information is available from the Wiley Online Library or from the author.

### Acknowledgements

This work was financially supported by the National Natural Science Foundation of China (Grant Nos. 12174123 and 12374347), the Natural Science Foundation of Guangdong Province, China (Grant No. 2022A1515010747), and Guangzhou Fundamental Science and Application Foundation (Grant No. 202201010445). The authors would like to thank Dr. Jiahao Yan in Jinan University for the help in the PL lifetime measurements.

## Conflict of Interest

The authors declare no conflict of interest.

## Data Availability Statement

The data that support the findings of this study are available from the corresponding author upon reasonable request.

## Keywords

charge transfer, dielectric-metal nanocavity, heterobilayer, photoluminescence, purcell factor, strain, transition metal dichalcogenide

Received: September 1, 2023

Revised: November 6, 2023

Published online:

- [1] B. Radisavljevic, A. Radenovic, J. Brivio, V. Giacometti, A. Kis, *Nat. Nanotechnol.* **2011**, *6*, 147.
- [2] K. F. Mak, J. Shan, *Nat. Photonics* **2016**, *10*, 216.
- [3] K. F. Mak, C. Lee, J. Hone, J. Shan, T. F. Heinz, *Phys. Rev. Lett.* **2010**, *105*, 136805.
- [4] A. Splendiani, L. Sun, Y. Zhang, T. Li, J. Kim, C.-Y. Chim, G. Galli, F. Wang, *Nano Lett.* **2010**, *10*, 1271.
- [5] H. S. S. Ramakrishna Matte, A. Gomathi, A. K. Manna, D. J. Late, R. Datta, S. K. Pati, C. N. R. Rao, *Angew. Chem. Int. Ed. Engl.* **2010**, *49*, 4059.
- [6] K. F. Mak, K. He, J. Shan, T. F. Heinz, *Nat. Nanotechnol.* **2012**, *7*, 494.
- [7] Q. H. Wang, K. Kalantar-Zadeh, A. Kis, J. N. Coleman, M. S. Strano, *Nat. Nanotechnol.* **2012**, *7*, 699.
- [8] H.-L. Liu, C.-C. Shen, S.-H. Su, C.-L. Hsu, M.-Y. Li, L.-J. Li, *Appl. Phys. Lett.* **2014**, *105*, 201905.
- [9] B. Zhu, X. Chen, X. Cui, *Sci. Rep.* **2015**, *5*, 9218.
- [10] Y. Li, A. Chernikov, X. Zhang, A. Rigosi, H. M. Hill, A. M. Van Der Zande, D. A. Chenet, E. N.-M. Shih, J. Hone, T. F. Heinz, *Phys. Rev. B* **2014**, *90*, 205422.
- [11] L. Xie, L. Wang, W. Zhao, S. Liu, W. Huang, Q. Zhao, *Nat. Commun.* **2021**, *12*, 5070.
- [12] L. Zhang, Z. Zhang, F. Wu, D. Wang, R. Gogna, S. Hou, K. Watanabe, T. Taniguchi, K. Kulkarni, T. Kuo, S. R. Forrest, H. Deng, *Nat. Commun.* **2020**, *11*, 5888.
- [13] C. Jin, E. C. Regan, A. Yan, M. Iqbal Bakti Utama, D. Wang, S. Zhao, Y. Qin, S. Yang, Z. Zheng, S. Shi, K. Watanabe, T. Taniguchi, S. Tongay, A. Zettl, F. Wang, *Nature* **2019**, *567*, 76.
- [14] D. i Huang, J. Choi, C.-K. Shih, X. Li, *Nat. Nanotechnol.* **2022**, *17*, 227.
- [15] W. Han, *APL Mater.* **2016**, *4*, 032401.
- [16] K. L. Seyler, P. Rivera, H. Yu, N. P. Wilson, E. L. Ray, D. G. Mandrus, J. Yan, W. Yao, X. Xu, *Nature* **2019**, *567*, 66.
- [17] B. Miller, A. Steinhoff, B. Pano, J. Klein, F. Jahnke, A. Holleitner, U. Wurstbauer, *Nano Lett.* **2017**, *17*, 5229.
- [18] X. Hong, J. Kim, S.-u.-F. Shi, Y. Zhang, C. Jin, Y. Sun, S. Tongay, J. Wu, Y. Zhang, F. Wang, *Nat. Nanotechnol.* **2014**, *9*, 682.
- [19] A. Karmakar, A. Al-Mahboob, C. E. Petoukhoff, O. Kravchyna, N. S. Chan, T. Taniguchi, K. Watanabe, K. M. Dani, *ACS Nano* **2022**, *16*, 3861.
- [20] M. Dandu, R. Biswas, S. Das, S. Kallatt, S. Chatterjee, M. Mahajan, V. Raghunathan, K. Majumdar, *ACS Nano* **2019**, *13*, 4795.
- [21] D. Kozawa, A. Carvalho, I. Verzhbitskiy, F. Giustiniano, Y. Miyauchi, S. Mouri, A. H. Castro Neto, K. Matsuda, G. Eda, *Nano Lett.* **2016**, *16*, 4087.
- [22] Y. Koo, Y. Kim, S. H. o Choi, H. Lee, J. Choi, D. Y. Lee, M. Kang, H. S. Lee, K. i K. Kim, G. Lee, K.-D. Park, *Adv. Mater.* **2021**, *33*, 2008234.
- [23] S. Li, K. a K. Chui, F. Shen, H. e Huang, S. Wen, C. Yam, L. Shao, J. Xu, J. Wang, *ACS Nano* **2022**, *16*, 10647.
- [24] C. Ma, J. Yan, Y. Huang, G. Yang, *Mater. Horiz.* **2019**, *6*, 97.
- [25] M. G. Harats, J. N. Kirchhof, M. Qiao, K. Greben, K. I. Bolotin, *Nat. Photonics* **2020**, *14*, 324.
- [26] Y. Gong, J. Lin, X. Wang, G. Shi, S. Lei, Z. Lin, X. Zou, G. Ye, R. Vajtai, B. I. Yakobson, H. Terrones, M. Terrones, B. K. Tay, J. Lou, S. T. Pantelides, Z. Liu, W. u Zhou, P. M. Ajayan, *Nat. Mater.* **2014**, *13*, 1135.
- [27] Y. Koo, H. Lee, T. Ivanova, A. Kefayati, V. Perebeinos, E. Khestanova, V. Kravtsov, K.-D. Park, *Light Sci. Appl.* **2023**, *12*, 59.
- [28] H. Shinomiya, H. Sugimoto, T. Hinamoto, Y. J. Lee, M. L. Brongersma, M. Fujii, *ACS Photonics* **2022**, *9*, 1741.
- [29] J. Sun, H. Hu, D. i Zheng, D. Zhang, Q. Deng, S. Zhang, H. Xu, *ACS Nano* **2018**, *12*, 10393.
- [30] X. Han, K. Wang, P. D. Persaud, X. Xing, W. Liu, H. Long, F. Li, B. Wang, M. R. Singh, P. Lu, *ACS Photonics* **2020**, *7*, 562.
- [31] J. Kern, A. Trügler, I. Niehues, J. Ewering, R. Schmidt, R. Schneider, S. Najmaei, A. George, J. Zhang, J. Lou, U. Hohenester, S. Michaelis De Vasconcellos, R. Bratschitsch, *ACS Photonics* **2015**, *2*, 1260.
- [32] M. Ringler, A. Schwemer, M. Wunderlich, A. Nichtl, K. Kürzinger, T. A. Klar, J. Feldmann, *Phys. Rev. Lett.* **2008**, *100*, 203002.
- [33] J. Cambiasso, M. König, E. Cortés, S. Schlücker, S. A. Maier, *ACS Photonics* **2018**, *5*, 1546.
- [34] S. Viarbitskaya, A. Teulle, R. Marty, J. Sharma, C. Girard, A. Arbouet, E. Dujardin, *Nat. Mater.* **2013**, *12*, 426.
- [35] N. J. Halas, S. Lal, W.-S. Chang, S. Link, P. Nordlander, *Chem. Rev.* **2011**, *111*, 3913.
- [36] T. K. Hakala, H. T. Rekola, A. I. Väkeväinen, J. - P. Martikainen, M. Necada, A. J. Moilanen, P. Törmä, *Nat. Commun.* **2017**, *8*, 13687.
- [37] N. Peimyoo, J. Shang, W. Yang, Y. Wang, C. Cong, T. Yu, *Nano Res.* **2014**, *8*, 1210.
- [38] Y. H. Fu, A. I. Kuznetsov, A. E. Miroshnichenko, Y. e F. Yu, B. Luk'yanchuk, *Nat. Commun.* **2013**, *4*, 1527.
- [39] Q. Zhao, J. i Zhou, F. Zhang, D. Lippens, *Mater. Today* **2009**, *12*, 60.
- [40] A. E. Miroshnichenko, Y. S. Kivshar, *Nano Lett.* **2012**, *12*, 6459.
- [41] A. B. Evlyukhin, S. M. Novikov, U. Zywietz, R. L. Eriksen, C. Reinhardt, S. I. Bozhevolnyi, B. N. Chichkov, *Nano Lett.* **2012**, *12*, 3749.
- [42] H. Huang, F. u Deng, J. Xiang, S. Li, S. Lan, *Appl. Surf. Sci.* **2021**, *542*, 148660.
- [43] S. Liu, F. u Deng, W. Zhuang, X. He, H. Huang, J.-D. Chen, H. Pang, S. Lan, *ACS Nano* **2022**, *16*, 14390.
- [44] Y. Meng, T. Wang, C. Jin, Z. Li, S. Miao, Z. Lian, T. Taniguchi, K. Watanabe, F. Song, S.-u.-F. Shi, *Nat. Commun.* **2020**, *11*, 2640.
- [45] K. e Wei, Y. u Liu, H. Yang, X. Cheng, T. Jiang, *Appl. Opt.* **2016**, *55*, 6251.
- [46] F. Cadiz, C. Robert, G. Wang, W. Kong, X. i Fan, M. Blei, D. Lagarde, M. Gay, M. Manca, T. Taniguchi, K. Watanabe, T. Amand, X. Marie, P. Renucci, S. Tongay, B. Urbaszek, *2D Mater.* **2016**, *3*, 045008.
- [47] Z. Yan, E. T. Poh, Z. Zhang, S. T. Chua, X. Wang, X. Wu, Z. Chen, J. Yang, Q.-H. Xu, K. E. J. Goh, R. Zhao, C.-H. Sow, *ACS Nano* **2020**, *14*, 5946.
- [48] U. Gosele, H. Stenzel, M. Reiche, T. Martini, H. Steinkirchner, Q. Y. Tong, *Solid State Phenom* **1996**, *47–48*, 33.
- [49] G. Lomboy, S. Sundararajan, K. Wang, S. Subramaniam, *Cem. Concr. Res.* **2011**, *41*, 1157.
- [50] H. Li, Y. Xu, J. Xiang, X. F. Li, C. Y. Zhang, S. L. Tie, S. Lan, *Nanoscale* **2016**, *8*, 18963.
- [51] J. Xiang, J. Chen, S. Lan, A. E. Miroshnichenko, *Adv. Opt. Mater.* **2020**, *8*, 2000489.
- [52] G. M. Akselrod, C. Argyropoulos, T. B. Hoang, C. Ciraci, C. Fang, J. Huang, D. R. Smith, M. H. Mikkelsen, *Nat. Photonics* **2014**, *8*, 835.

- [53] L. Su, Y. Yu, L. Cao, Y. Zhang, *Nano Res.* **2015**, *8*, 2686.
- [54] H. Lee, Y. Koo, S. Kumar, Y. Jeong, D. G. Heo, S. H.o Choi, H. Joo, M. Kang, R. H. Siddique, K.i K. Kim, H. S. Lee, S. An, H. Choo, K.-D. Park, *Nat. Commun.* **2023**, *14*, 1891.
- [55] C.-Q. Li, C.-Y. Zhang, Z.-S. Huang, X.-F. Li, Q.-F. Dai, S. Lan, S.-L. Tie, *J. Phys. Chem. C* **2013**, *117*, 24625.
- [56] P. B. Johnson, R. W. Christy, *Phys. Rev. B* **1972**, *6*, 4370.
- [57] F.u Deng, H. Huang, J.-D. Chen, S. Liu, H. Pang, X. He, S. Lan, *Nano Lett.* **2022**, *22*, 220.
- [58] M. Pollnau, M. Eichhorn, Emission Cross Section, Fuchtbauer-Ladenburg Equation, and Purcell Factor, Springer Netherlands, Dordrecht **2017**.
- [59] S. Huang, T. Ming, Y. Lin, X.i Ling, Q. Ruan, T. Palacios, J. Wang, M. Dresselhaus, J. Kong, *Small* **2016**, *12*, 5190.